Synthesis and characterization of $\{Mo_{72}Fe_{30}\}$-coated large hexagonal gibbsite γ-$Al(OH)_3$ platelets†

Soumyajit Roy,*‡ Hans J. D. Meeldijk, Andrei V. Petukhov, Marjan Versluijs and Fouad Soulimani

Received 14th January 2008, Accepted 13th March 2008
First published as an Advance Article on the web 15th April 2008
DOI: 10.1039/b800680f

The polyoxometalates or POMs (clusters comprising at least two metal and many oxygen atoms) have recently gained significant interest owing to their versatile architecture and especially their catalytic activities. Due to their high catalytic activity but low surface area, there is always a demand for making high surface area POMs. This work demonstrates the attachment of the anionic $\{Mo_{72}Fe_{30}\}$ POMs to gibbsite nanoplatelets with a residual positive charge to form large surface area composites. The resulting composite reported here has been characterized using cryo-TEM imaging, EDX/STEM (elemental) analysis, ATR-IR spectroscopy, SAXS, electrophoretic mobility determination and XRD. The composite reported here could find application in catalysis.

Introduction

Polyoxometalates (POMs) are a class of clusters comprising of multiple single/mixed-valent metal centres, each of whose coordination requirements are fulfilled by water/ligand molecules.[1] They have been extensively studied mainly because of their attractive catalytic properties, for instance in the oxidation of aldehydes, CO, oxidative dehydrogenation, *etc.*[2,3] Owing to their high catalytic activity, but low surface area (usually around 1–10 $m^2\ g^{-1}$) there has always been a demand for making high surface area POMs. To achieve that goal, smaller POMs like Keggins have been placed between pillared clays or layered double hydroxides, molecular sieves MCM-41, polyaniline and poly-pyrrole films,[4] and even very recently on silica nanoparticles.[5] They have also been placed on highly oriented, pyrolytic graphite surfaces by the technique of so-called 'solvent casting' and investigated by scanning tunneling microscopy/spectroscopy (STM/STS).[6] A recent development in the field has been made with the synthesis of a family of unusually large, protein-like, discrete single molecular clusters by exploiting a 'virtual library' of pentagonal building blocks abundant in the solution.[7] Examples include: $\{Mo_{132}\}$, $\{Mo_{368}\}$, $\{Mo_{72}Fe_{30}\}$ *etc.* Of these, the last cluster, $\{Mo_{72}Fe_{30}\}$ (or more precisely $\{Mo_{72}Fe_{30}(H_2O)_{30}O_{252}L_{12}\}\cdot ca.150H_2O$ where $L = H_2O$, CH_3COO, $Mo_2O_{8/9}$) though it has a very high stability, self-assembles spontaneously to form blackberry-like structures in solution.[8,9] (Note: this cluster will be referred to from here onwards as $\{Mo_{72}Fe_{30}\}$ for convenience.) It would hence in principle be interesting to design, in a controlled way, a large surface area material based on newly characterized large POMs like $\{Mo_{72}Fe_{30}\}$. A possible route to realizing such a directed design of stable, high surface area $\{Mo_{72}Fe_{30}\}$-based materials would mean using colloidal scaffolds of complementary charge. In our laboratory, high surface area, plate-like, colloidal gibbsite nanoparticles (85 $m^2\ g^{-1}$) have been developed and their synthesis optimized.[10]

Gibbsite templated hexagonal silica platelets[11] and fluorescent platelets[12] have also been prepared. For a high surface area $\{Mo_{72}Fe_{30}\}$-based material we hence chose gibbsite platelets as scaffolds. The complementarity of charge between $\{Mo_{72}Fe_{30}\}$ and gibbsite further prompted this choice. This charge complementarity can be understood as follows. The pH of discrete $\{Mo_{72}Fe_{30}\}$ clusters upon dissolution in water is around 4.5 whereas the isoelectric point or rather the point of zero charge of gibbsites is quite high, around pH 10.1. Hence, at a pH of around 4.5, the surface of the gibbsite nanocrystal is expected to be positively charged, (based on the following equilibrium[13]), which in turn could act as a suitable platform for the attachment of anionic $\{Mo_{72}Fe_{30}\}$ clusters:

$$Al\text{–}OH_2^+ + H_2O \rightleftharpoons Al\text{–}OH + H_3O^+$$

Consequently at a pH of 4.5, complementary charges on gibbsite nanocrystals and $\{Mo_{72}Fe_{30}\}$ clusters could act as glue for binding the latter on the surface of the former to form hexagonal platelets of $\{Mo_{72}Fe_{30}\}$ clusters, the basic strategy of our synthesis. (Fig. 1)

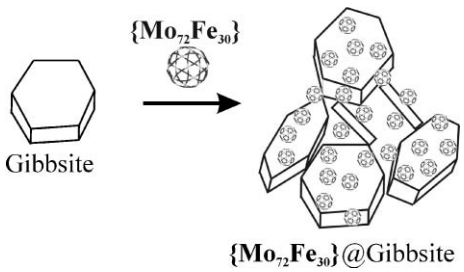

Fig. 1 Schematic representation of the reaction leading to the formation of hexagonal platelets of the gibbsite@$\{Mo_{72}Fe_{30}\}$ composite. A network of the composite platelets in the composite gel is implied (see text for details); however, no inference should be drawn regarding the arrangement of the $\{Mo_{72}Fe_{30}\}$ on the platelets of the composite from this schematic diagram.

Van't Hoff Laboratory for Physical and Colloid Chemistry, Debye Institute and Electron Microscopy Department of Molecular Cell Biology, University of Utrecht, Padualaan 8, 3584 CH, Utrecht, The Netherlands. E-mail: s.roy@isis.u-strasbg.fr; Fax: +31 (0)30 253 3870

† Electronic supplementary information (ESI) available: Colour version of Fig. 2. See DOI: 10.1039/b800680f

‡ Present address: BASF-ISIS, Strasbourg, France

In this article the synthesis and the characterization of the composite $\{Mo_{72}Fe_{30}\}$@gibbsite is described in detail. In principle, changing the template topology (in this case, the plate-like gibbsite) would enable us to change the shape of the desired mesoscopic polyoxometalate. The experimental detail of the work is described in the following section.

Experimental

Synthetic method

To a colloidal dispersion of 10 ml gibbsite platelets (12 g l^{-1}) prepared according to ref. 10, 25 mg of $\{Mo_{72}Fe_{30}\}$ was added. (Note: $\{Mo_{72}Fe_{30}\}$ was prepared by addition of 1.1 g of $FeCl_3$ to 75 ml of an aqueous acidic solution of 1.4 g of ammonium salt of $\{Mo_{132}\}$ and 1.3 g of sodium acetate trihydrate, and the solution was then allowed to crystallize. The crystals were collected and used for our synthesis. For details on this synthetic method refer to ref. 1*c* and 16.) The resulting dispersion was stirred for 1 h. The pH of the dispersion was 4.5. The faintly blue dispersion formed a light-yellow gel in the course of stirring. It was allowed to stand for 3 h. The dense gel phase separated (Fig. 2). The dense phase of the gel rich in the composite was characterized *in situ* and also in the dried state using transmission electron microscopy (TEM), cryo-TEM imaging, energy-dispersive X-ray/scanning transmission electron microscopy with a high-angle annular dark-field detector [EDX/STEM-HAADF (elemental) analysis], attenuated total-reflection infraread (ATR-IR), Fourier-transform infrared (FTIR) and Raman spectroscopy, small-angle X-ray scattering (SAXS), electrophoretic mobility determination and X-ray diffraction (XRD) experiments as described below.

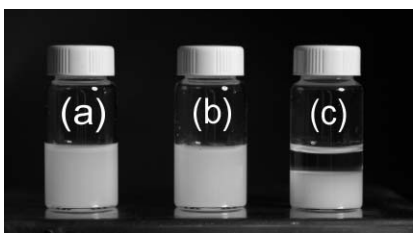

Fig. 2 (a) Starting (bluish) gibbsite dispersion; (b) changes colour (yellow) after the addition of crystals of $\{Mo_{72}Fe_{30}\}$ to the dispersion and stirring; (c) finally leading to the composite $\{Mo_{72}Fe_{30}\}$@gibbsite as a (yellow) gel at the bottom. The colour version of this Figure is freely available as ESI.†

Characterization of the composite

Cryo-transmission electron microscopy and EDX/STEM. The characterization of the $\{Mo_{72}Fe_{30}\}$–gibbsite composite was primarily done by the use of a Tecnai 20 (FEI Company) transmission electron microscope operated at an accelerating voltage of 200 kV. At least 1000 particles were imaged and nearly all of them revealed corrugations on edges and surfaces. Further confirmation was carried out by EDX/STEM-HAADF (energy-dispersive X-ray/scanning transmission electron microscopy with a high-angle annular dark-field detector) using a Tecnai 20 EDX/TEM detector. The cryo-TEM images were also obtained using the same microscope with the use of a Gatan cryo-holder. The TEM micrographs have been processed using SIS software (Soft Imaging System) and the EDX spectra were acquired using TIA software (Tecnai imaging and analysis software).

ATR-FTIR spectroscopy. ATR-FTIR measurements were carried out at room temperature on a Perkin-Elmer 2000 Fourier-transform spectrometer equipped with a DTGS detector. Spectra were recorded with an ATR accessory (PIKE) equipped with a diamond crystal as the reflecting element. Data-point resolution of the spectra was 4 cm^{-1} and 10 scans were accumulated for one spectrum. Spectral interpretation was carried out after subtraction of the spectrum of water as background.

Raman spectroscopy. Raman spectroscopic measurements were carried out on a Kaiser RXN spectrometer equipped with a 50 mW, 532 nm diode laser for excitation, a holographic grating for dispersion and a Peltier-cooled Andor CCD camera for detection. Spectra were recorded in glass vials at room temperature. Detector pixel resolution was about 2 cm^{-1} and 10 scans were accumulated for one spectrum at an exposure time of 20 s per scan.

Electrophoretic mobility. The electrophoretic mobilities were measured using dilute samples of gibbsite and $\{Mo_{72}Fe_{30}\}$–gibbsite composite by Coulter DELSA 440 SX in water at a pH of *ca.* 5.5, and a temperature of 298 K. The electrophoretic mobilities of the composite and gibbsite were found to be +0.3 and + 5.5 [$\mu m\ cm\ s^{-1}\ V^{-1}$] respectively.

X-Ray diffraction experiments. XRD measurements were carried out on a D8 theta–theta system from Bruker AXS in Bragg–Brentano geometry, automatic divergency slit (6 mm for the composite and gibbsite; 20 mm for $\{Mo_{72}Fe_{30}\}$), 2.5° Soller slits, Co $K\alpha_{1,2}$ radiation ($\lambda = 1.79026$ Å).

Small-angle X-ray scattering experiments. The SAXS experiments were carried out at the Dutch–Belgian beam line BM-26 (DUBBLE) of the European Synchrotron Radiation Facility (ESRF) in Grenoble (France).[14] The X-ray beam with photon energy of 11 keV (wavelength 0.11 nm) was used. To improve angular resolution, the beam was focused at the detector position located at about 8 m from the sample as described in more detail in the literature.[15] The data was collected using a gas-filled detector (512 × 512 pixels of 255 μm^2) and a CCD-based Photonic Science detector (4008 × 2671 pixels of 22 μm^2). The measurements are performed for pure solvent (water), of the composite and a comparable concentration of the gibbsite dispersion. The reported data has been corrected for the background (measured from a capillary filled with distilled water). The radial intensity profiles are (orientationally) averaged results of measurements with the CCD detector (0.013 $nm^{-1} < q < 0.38\ nm^{-1}$) and the larger gas-filled detector (0.2 $nm^{-1} < q < 1.2\ nm^{-1}$).

Results and discussion

The gibbsite suspension used as a starting material is almost colorless. Strictly speaking the starting dispersion is faintly turbid and has a slight bluish tinge which reflects the length scales of its constituent hexagonal platelets. (Note: the color is due to scattering of light by its components, the platelets.) However, upon addition of crystals of discrete $\{Mo_{72}Fe_{30}\}$-type clusters (prepared according to ref. 16) to the dispersion of gibbsite, the colour of the dispersion changes to light yellow (the colour of $\{Mo_{72}Fe_{30}\}$)

and upon standing (approx. for 3 h) the composite material settles down forming a gel (Fig. 2); the pH of the dispersion was measured to be 4.5. Clearly the formation of the gel created an additional problem in the characterization of the composite. However, such a gelation is expected taking into account the fact that the gibbsite dispersion itself is positively charge stabilized and, on attachment of anionic $\{Mo_{72}Fe_{30}\}$, our desired material is formed as a gel due to the charge neutralization of the gibbsites in the composite.

Analyzing the composite

1. TEM, cryo-TEM imaging and STEM/EDX. A part of the $\{Mo_{72}Fe_{30}\}$–gibbsite composite was taken out and re-dispersed in water and a drop of that dispersion was dried and imaged by TEM. The TEM image of the composite revealed clear corrugations and darkened edges as compared to the sharp and smooth edge of a pristine gibbsite nanocrystal and a 'mottled' surface rather than the immaculate surface of a templating gibbsite, implying its 'coverage' by the negatively charged $\{Mo_{72}Fe_{30}\}$. However, due to the gel-like nature of the composite it was necessary to have an insight into the structure of the system in its native (not dried) state. The gel was investigated by cryo-TEM, by plunge freezing the gel of the composite to a temperature of 90 K. The cryo-TEM images (Fig. 3) show two interesting features. First, it shows additional dark spots on the otherwise smooth surface of the gibbsite platelets and additionally a network-type arrangement of platelets with some face-to-edge contacts. The dark spots are of the diameter of around 2–3 nm and are compatible with the diameter of a single molecular $\{Mo_{72}Fe_{30}\}$ cluster and they hence imply attachment of the negative $\{Mo_{72}Fe_{30}\}$ clusters on the surface of the positively charge-stabilized gibbsite, ultimately leading to the formation of a neutral composite. These (neutral) composites then arrange like a 'house of cards' network—the microscopic picture of the gel in its native state. (Fig. 3)

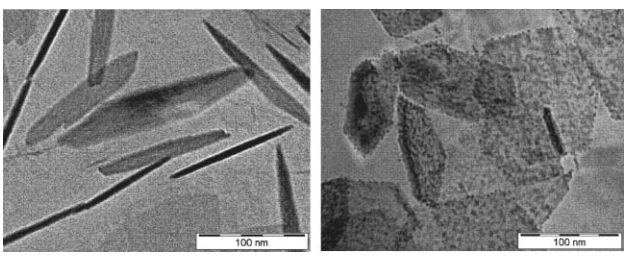

Fig. 3 Cryo-TEM images of starting gibbsite platelets (left) and the gibbsite–$\{Mo_{72}Fe_{30}\}$ composite (right). The dark spots on the gibbsite platelets in the right-hand image reveals the $\{Mo_{72}Fe_{30}\}$ clusters. Note no such spots are there on pure gibbsite on the left. Also note the network-like arrangement of the composites on the right-hand side. The scale bar indicates 100 nm.

For a more quantitative picture, EDX and STEM-HAADF analyses were carried out on the surface of the $\{Mo_{72}Fe_{30}\}$–gibbsite composite in the dried state. The EDX experiments coupled with a STEM-HAADF detector consistently reveal a ratio of Mo : Fe of around 2.6 : 1. From the reported crystal structure of the cluster $\{Mo_{72}Fe_{30}\}$, the Mo : Fe ratio is calculated to be 2.4 : 1. The agreement is quantitative and implies the presence of the clusters on the surface of the gibbsite platelets (Fig. 4). Although

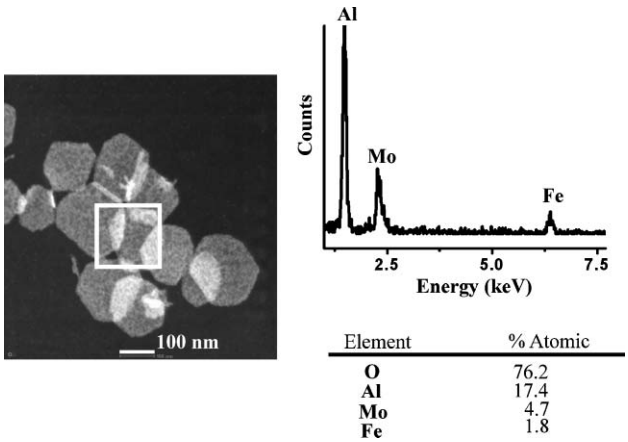

Element	% Atomic
O	76.2
Al	17.4
Mo	4.7
Fe	1.8

Fig. 4 A representative STEM-HAADF image of the composite (left) together with EDX spectrum of the composite. (The square box in the left image denotes the region where the EDX analysis has been carried out.) The numerical values for atomic abundance of respective elements have been tabulated. In the EDX spectrum the abundance of oxygen has been omitted for clarity.

the presence of the $\{Mo_{72}Fe_{30}\}$ on the cluster surface was apparent from cryo-TEM and the combination of STEM and EDX, we did not succeed in obtaining high-resolution TEM (HRTEM) images of the composite. The failure to obtain HRTEM apparently resulted because of the liquid-like distribution of the $\{Mo_{72}Fe_{30}\}$ clusters on the gibbsite surface. (The indication of absence of any regular periodic structure on the surface of the composite was further shown by powder XRD experiments described later.)

2. SAXS measurements. To investigate the structure of the composites in solution, SAXS measurements were carried out. It is known that the gibbsite platelets can form ordered nematic or columnar phases, leading to pronounced features in the SAXS domain, due to positional correlations between the constituent platelets in liquid state; this has been shown recently in our laboratory.[17,18] The results of the SAXS study with our composite and bare gibbsite are presented in Fig. 5. No significant difference in the scattering patterns is discernable. No remarkable positional

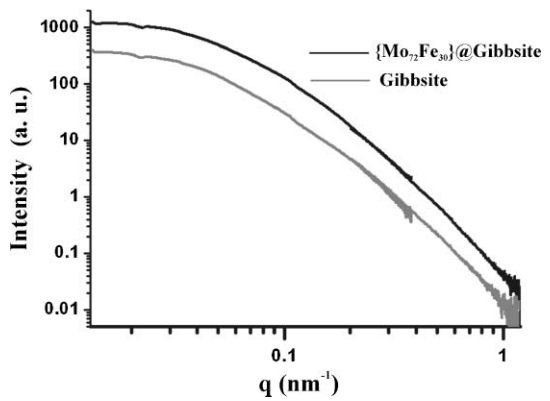

Fig. 5 The SAXS pattern of the gibbsite and that of the composite is depicted. No significant difference is observed in the scattering patterns. The higher intensity with the composite apparently stems from the higher concentration of the particles in the composite. However, no long-range positional correlations are observed and hence the TEM view of a network-type structure in the composite is upheld.

correlation between the gibbsite platelets in the composite is observed. This excludes the presence of ordered structures such as those in the nematic or columnar phases, and upholds the structure of a network of platelets in the composite as observed from TEM.[17,18] Furthermore, no additional feature due to the $\{Mo_{72}Fe_{30}\}$ clusters was detected. Presumably the contribution of these small clusters to the SAXS data in Fig. 5 is far too weak. We were therefore unable to find any information on the positional correlation between them on the gibbsite surface and hence no detailed information on the structure of the interface could be obtained.

3. XRD. In order to have information on the structure of the interface of the composite, a part of the composite was dried and analysed with XRD. In comparison to the pure gibbsite, XRD of the composite showed a broad 'hump' (in the range of $2\theta = 30$–$40°$), which originates from $\{Mo_{72}Fe_{30}\}$ clusters (see the spectrum of pure $\{Mo_{72}Fe_{30}\}$). We also note the absence of any clear inter-cluster correlations peaks in this 2θ region, which implies a disordered disposition of the $\{Mo_{72}Fe_{30}\}$ clusters on the surface of the gibbsite platelets in the composite (Fig. 6). In other words it implies a liquid-like disposition of the $\{Mo_{72}Fe_{30}\}$ clusters on the surface of the gibbsite platelets in the composite, which perhaps led to an increase in the scattering intensity and a broadening of the scattering pattern of the composite in the said 2θ regime (Fig. 6). Note: by liquid-like we mean a disordered disposition, *i.e.* there is no crystalline long-range order but there is an occasional presence of short-range locally ordered domains as in liquids.

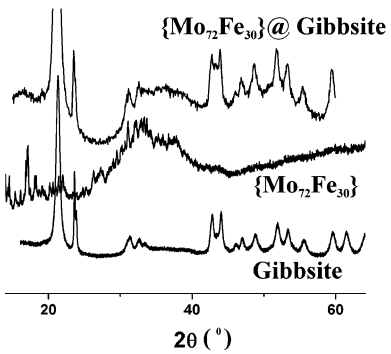

Fig. 6 Comparative XRDs of gibbsite, $\{Mo_{72}Fe_{30}\}$ and the $\{Mo_{72}Fe_{30}\}$–gibbsite composite.

4. Attenuated total-reflection IR (ATR-IR) spectroscopy and Raman spectroscopy. ATR-IR spectra (Fig. 7) of the composite show interesting features. In the range of 600–1200 cm^{-1} the spectrum of the composite shows bands characteristic of both gibbsite and $\{Mo_{72}Fe_{30}\}$ clusters, implying successful attachment of the latter on the surface of the gibbsite in the composite, in its native, non-dried solution state. Raman spectroscopy reconfirms this observation. Additionally we note that although the concentration of gibbsite is much higher in the composite gel phase than the starting gibbsite concentration, yet the intensity of the bands in the ATR-IR spectrum of the composite in the range of 3200–3700 cm^{-1} (characteristic for ν_{OH}) is higher than that of those in the gibbsite (Fig. 8).

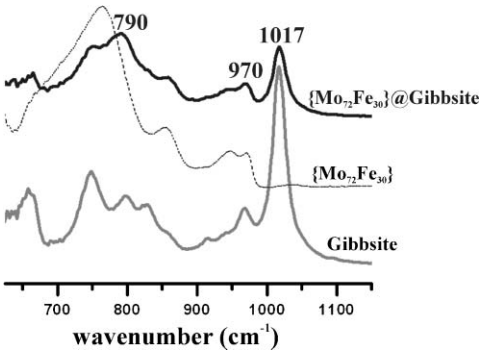

Fig. 7 ATR-IR spectra of gibbsite, $\{Mo_{72}Fe_{30}\}$ and the composite. (The intensities of the spectra are not to scale.)

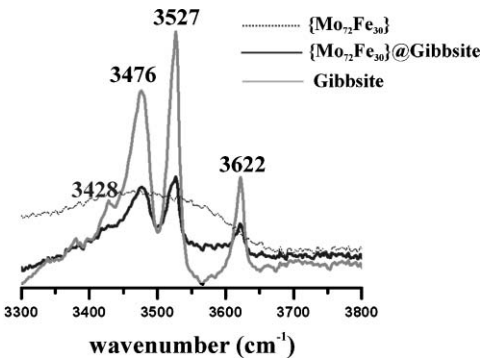

Fig. 8 ATR-IR spectra of the gibbsite, $\{Mo_{72}Fe_{30}\}$ and the composite showing the characteristic bands for ν_{OH}. Note the apparently anomalous alterations in the band intensities in the course of the formation of the composite.

The four ν_{OH} bands in this regime (Fig. 8) in gibbsite have been attributed to represent the surface structure of gibbsite.[19] Hence, the observed alteration in the intensity of those bands in the composite with respect to the starting gibbsite can be interpreted as a signature of the alteration of the surface structure of the gibbsite in the composite. In other words we might say that $\{Mo_{72}Fe_{30}\}$ clusters in the composite alter/induce disorder on the surface of the hexagonally close-packed hydroxyl groups on the gibbsite surface and thereby alter the intensity of the ν_{OH} bands in the spectra of the composite. (Note: similar vibrational spectroscopic features were observed from the dried composite.)

5. Electrophoretic mobility measurements. The gibbsite nanocrystal is positively charged at the pH (4.5) of our reaction. This is so because the pH (4.5) of the reaction is much lower than the isoelectric point of gibbsite (pH ~10.1)[13] and hence according to the following equilibrium the nanocrystal surface is positively charged.

$$Al\text{–}OH_2^+ + H_2O \rightleftharpoons Al\text{–}OH + H_3O^+$$

The positive surface charge is reflected in the electrophoretic mobility of the gibbsite platelets which is determined to be 5.5 μm cm V^{-1} s^{-1} (see also ref. 13). However, upon the formation of the composite gel the electrophoretic mobility is reduced to 0.3 μm cm V^{-1} s^{-1}. It implies compensation of the positive surface charge of the gibbsite platelet due to its coverage by negatively charged $\{Mo_{72}Fe_{30}\}$ clusters.

Hence from the above set of experimental observations we could infer that using colloidal gibbsite platelets with residual positive surface charge we have successfully synthesized hexagonal composite platelets of $\{Mo_{72}Fe_{30}\}$ on gibbsite. Although the exact nature of the interface structure could not be obtained, the composite demonstrates the possibility of designing mesoscopic large surface area polyoxometalates, using colloidal scaffolds (like gibbsites as used in this case). Here colloidal gibbsite platelets are used as structure-directing agents to avoid the complex chemical labyrinth, an obstacle towards mesoscopic POM design. In principle, any charge-stabilized colloidal particle can be used as a structure-directing agent for making engineered POMs as the composite described here. We may hence further propose to refer to this technique of using a colloidal particle as a template for forming large surface area POMs as 'colloidal casting'. The requirements for successful colloidal casting might be summarized as follows: complementarities of charge between the colloidal templates and the POM to be templated (as mentioned above, here it is between the positively charged gibbsite platelets and anionic POMs). (It is also to be noted that there is a significant difference in the matter of the chemistry of the edges and faces of the gibbsite nanocrystal and hence nonuniformity in distribution of the $\{Mo_{72}Fe_{30}\}$ clusters might take place as well.) A common solvent for both the components for effective templating (here water) is indeed necessary.

Conclusions

In this article, we demonstrate that it is possible to 'glue' larger POMs like the $\{Mo_{72}Fe_{30}\}$ clusters on the surface of gibbsite platelets to form large-surface hexagonal POM platelets in an engineered yet facile manner. (Note: the $\{Mo_{72}Fe_{30}\}$ clusters in dilute aqueous dispersion spontaneously form self-assembled superstructures and the reason why such structures are formed is still not known.) Additionally, it is still a challenge to predict and control the cluster size and morphology of POMs in the mesoscopic regime (in the range of 100–900 nm) since it is difficult to maneuver the interplay of chemistry of multiple metal centers, pH and the redox state of the complete system. This technique of 'colloidal casting', as it may be called, can be crucial since it bypasses the complex chemical crossroad and resorts to the use of preformed colloidal entities as templates/scaffolds for an engineered design of a mesoscopic POM architecture. The technique is evidently supramolecular (in the sense that it involves supramolecular electrostatic and induced-dipole interactions way beyond the chemistry of molecules), and it also provides a platform to 'glue' molecules to form mesoscopic supramolecular architecture. As a second step, a simple condensation reaction can be thought of between the $\{Mo_{72}Fe_{30}\}$ clusters on the surface of the composite reported here. The possibility of using such high surface area composites as reported here can potentially pave the path for the ongoing search of high surface area POMs for catalytic applications. Additionally it is perhaps further worth mentioning that Co- or Mo-impregnated alumina is used as a hydrodesulfuration (HDS) catalyst, where the loss of Co is a long-standing problem.[20] The Co analogue of the complex $\{Mo_{72}Fe_{30}\}$ immobilized on gibbsite prepared in a fashion similar to that reported here could serve as an important HDS catalyst. By substituting Fe with Co in our composite, a HDS catalyst might be made.

Acknowledgements

We thank W. K. Kegel for helpful discussion, encouragement, support and critical reading of the manuscript. Thanks are due to H. N. W. Lekkerkerker, Maurice C. D. Mourad, J. W. Geus, A. P. Philipse, J. Groenewold, and S. Sacanna for helpful discussion. A. Imhof, J. H. J. Thijssen, D. C. 't Hart as well as the personnel of the DUBBLE beam-line are thanked for their help during the SAXS measurements. The beam-time was provided by NWO. This research was financially supported by NWO-CW.

References

1 (*a*) M. T. Pope, *Heteropoly and Isopoly Oxometalates*, Springer, Berlin, 1983; (*b*) Thematic issue on polyoxometalates, ed. C. L. Hill, *Chem. Rev.*, 1998, **98**; (*c*) A. Müller, S. K. Das, E. Krickemeyer and C. Kuhlmann, *Inorg. Synth.*, 2004, **34**, 191–200; (*d*) M. T. Pope and A. Müller, *Angew. Chem., Int. Ed. Engl.*, 1991, **30**, 34–38; (*e*) T. Liu, E. Diemann and A. Müller, *J. Chem. Educ.*, 2007, **3**, 526–532.
2 N. Mizuno and M. Misono, *Chem. Rev.*, 1998, **98**, 199–217.
3 C. L. Hill and C. M. Prosser-McCartha, *Coord. Chem. Rev.*, 1995, **143**, 407–455.
4 For a review on the topic see: I. V. Kozhevnikov, *Chem. Rev.*, 1998, **98**, 171–198.
5 (*a*) N. M. Okun, T. M. Anderson and C. L. Hill, *J. Am. Chem. Soc.*, 2003, **125**, 3194–3195; (*b*) N. M. Okun, M. D. Ritorto, T. M. Anderson and C. L. Hill, *Chem. Mater.*, 2004, **16**, 2551–2558; (*c*) for an overview on core-shell templating, see: F. Caruso, *Adv. Mater.*, 2001, **13**, 11–22.
6 I. K. Song, M. S. Kaba, G. Coulston, K. Kourtakis and M. A. Barteau, *Chem. Mater.*, 1996, **8**, 2352–2358.
7 (*a*) A. Müller and C. Serain, *Acc. Chem. Res.*, 2000, **33**, 2–10; (*b*) A. Müller and S. Roy, *Coord. Chem. Rev.*, 2003, **245**, 153–166.
8 T. Liu, *J. Am. Chem. Soc.*, 2003, **125**, 312–313.
9 For an overview, see: A. Müller and S. Roy, *Eur. J. Inorg. Chem.*, 2005, 3561–3570.
10 J. E. G. J. Wijnhoven, *J. Colloid Interface Sci.*, 2005, **292**, 403–409.
11 J. E. G. J. Wijnhoven, *Chem. Mater.*, 2004, **16**, 3821–3828.
12 C. Vonk, S. M. Oversteegen and J. E. G. J. Wijnhoven, *J. Colloid Interface Sci.*, 2005, **287**, 521–525.
13 A. M. Wierenga, T. A. J. Lenstra and A. P. Philipse, *Colloids Surf., A*, 1998, **134**, 359–371.
14 W. Bras, I. P. Dolbnya, D. Detollenaere, R. van Tol, M. Malfois, A. J. Ryan and E. Heeley, *J. Appl. Crystallogr.*, 2003, **36**, 791–794.
15 A. V. Petukhov, I. P. Dolbnya, D. G. A. L. Aarts and G. J. Vroege, *Phys. Rev. E: Stat. Phys., Plasmas, Fluids, Relat. Interdiscip. Top.*, 2004, **69**, 031405.
16 A. Müller, S. Sarkar, S. Q. N. Shah, H. Bögge, M. Schmidtmann, Sh. Sarkar, P. Kögerler, B. Hauptfleisch, A. X. Trautwein and V. Schünemann, *Angew. Chem., Int. Ed.*, 1999, **38**, 3238–3241.
17 D. von der Beek, A. V. Petukhov, S. M. Oversteegen, G. J. Vroege and H. N. W. Lekkerkerker, *Eur. Phys. J. E*, 2005, **16**, 253–258.
18 A. V. Petukhov, D. von der Beek, R. P. A. Dullens, I. P. Dolbnya, G. J. Vroege and H. N. W. Lekkerkerker, *Phys. Rev. Lett.*, 2005, **95**, 214502.
19 H. D. Ruan, R. L. Frost and J. T. Kloprogge, *J. Raman Spectrosc.*, 2001, **32**, 745–750.
20 A. Corma, *Chem. Rev.*, 1997, **97**, 2373–2419.